^{103}Rh NMR Chemical Shifts in Organometallic Complexes: A Combined Experimental and Density Functional Study

Laura Orian,[a] Annalisa Bisello,[a] Saverio Santi,*[a] Alberto Ceccon,*[a] and Giacomo Saielli[b]

Abstract: Experimental ^{103}Rh NMR chemical shifts of mono- and binuclear rhodium(I) complexes containing *s*- or *as*-hydroindacenide and indacenediide bridging ligands with different ancillary ligands (1,5-cyclooctadiene, ethylene, carbonyl) are presented. A protocol, based on density functional theory calculations, was established to determine ^{103}Rh NMR shielding constants in order to rationalise the effects of electronic and structural variations on the spectroscopic signal, and to gain insight into the efficiency of this computational method when applied to organometallic systems. Scalar and spin–orbit relativistic effects based on the ZORA (zeroth order regular approximation) level have been taken into account and discussed. A good agreement was found for model compounds over a wide range of chemical shifts of rhodium ($\approx$10000 ppm). This allowed us to discuss the experimental and calculated $\delta(^{103}\mathrm{Rh})$ in larger complexes and to relate it to their electronic structure.

Keywords: bridging ligands · density functional calculations · NMR spectroscopy · rhodium

Introduction

The importance of rhodium complexes in homogeneous catalysis is widely documented.[1] Rhodium and, in general, the transition metals of Group VIII are also amenable to application in a novel research field which has attracted considerable attention in the last decade, that is, the construction of molecule-sized electronic components,[2] in which the electronic and chemical interactions between ligand-bridged metal groups can be finely tuned for potential applications, such as switches, current rectifiers and wires.

A rationale of possible correlations between structure and reactivity, or structure and catalytic activity, remains a challenging problem and clearly requires an accurate insight into the molecular and electronic structure, usually obtained by traditional approaches in organometallic chemistry through X-ray diffraction and molecular orbital (MO) calculations. The use of transition-metal NMR chemical shifts for a particular metal ion is another potentially effective working tool when structural/chemical properties of metal compounds are studied.[3] However, there are some difficulties in the experimental detection of a ^{103}Rh chemical shift due to the extremely low gyromagnetic ratio of a ^{103}Rh nucleus (natural abundance = 100 %, $I = 1/2$, $\gamma = -0.8420 \times 10^7\,\mathrm{rad\,T^{-1}\,s^{-1}}$) and its consequent low sensitivity (about 0.2 % that of ^{13}C). Nevertheless, a receptivity of about 20 % that of ^{13}C is obtained by using reverse-detection techniques,[4] such as heteronuclear multiple bond correlation (HMBC), in which the directly detected nucleus is the proton, in cases where ^{103}Rh is spin–spin coupled to ^{1}H.

Some of us have explored classes of multisite bridging ligands, that is, fulvalenyl and indenyl spacers, suitable for the construction of homo- and hetero-bimetallic model complexes, through which electronic communication can be investigated.[5] Recently, we synthesised monometallic rhodium derivatives of *s*- and *as*-hydroindacenide and bimetallic rhodium complexes of *s*- and *as*-indacenediide.[6] Other research groups studied homo-binuclear complexes of Fe, Co, Ni and Mn, with the same aromatic 14-π-electron spacers[7] that have been identified as suitable bridging ligands in view of the strong electronic interactions between the two coordinated metal centres. Moreover, their structure assures a control of the distance and orientation between the metal centres, which may be arranged in a *syn* or *anti* configuration with respect to the rigid bridge plane.

Several research groups have investigated the possibility of employing ^{103}Rh NMR as a probe to detect the thermodynamic stability of the complexes and predict their catalytic

[a] Dr. L. Orian, Dr. A. Bisello, Prof. S. Santi, Prof. A. Ceccon
Dipartimento di Scienze Chimiche
Università degli Studi di Padova
Via Marzolo 1, 35131 Padova (Italy)
E-mail: S.Santi@chfi.unipd.it
alberto.ceccon@unipd.it

[b] Dr. G. Saielli
Istituto per la Tecnologia delle Membrane del CNR
Sezione di Padova, Via Marzolo 1, 35131 Padova (Italy)

Supporting information for this article is available on the WWW under http://www.chemeurj.org/ or from the author.

 DOI: 10.1002/chem.200305671

activity. Quantitative studies on the correlation between $\delta(^{103}Rh)$ and the rate of CO/PPh_3 ligand exchange in $[Rh(Cp)(CO)_2(X)]$ were carried out by Von Philipsborn and co-workers, who found that the observed kinetic constants vary by up to four orders of magnitude in complexes with a chemical-shift variation of 200 ppm.[8] Öhrström found a linear correlation of $\delta(^{103}Rh)$ with thermodynamic stability constants for the replacement of one ethylene in $[Rh(acac)(C_2H_4)_2]$ (acac = 2,4-pentanedionate) with different olefins, such as propene, *cis*- and *trans*-butene.[9] The link between the stability of transition-metal complexes and catalytic activity depends in this case on the ease of the ligand exchange, which is favoured by metal deshielding. The review by Von Philipsborn[10] describes a recent state of the art application in which transition-metal nuclear magnetic spectroscopy is used to probe possible correlations between structure and reactivity in organometallic complexes.

Quantum-chemical calculations of the chemical shift of rhodium may be of great help in rationalising the experimental findings. The method needs to be flexible enough to cover the wide range of chemical shifts of ^{103}Rh ($\approx$12000 ppm). In addition, because rhodium belongs to the second transition row, the presence of relativistic effects has to be carefully investigated. In this respect, ab initio methods are not an option because of the high demand in computational resources, especially if large mono- and bimetallic complexes have to be investigated. Instead, density functional theory (DFT)[11] has proven to be very successful for the calculation of NMR properties of various nuclei.[12] In particular, the relativistic treatment implemented by the software code ADF (Amsterdam Density Functional)[13] allows the calculation of NMR properties of heavy atoms, with the possibility of using only scalar relativistic corrections, or to also consider the spin–orbit coupling.[14] Recently, a few computational investigations of the ^{103}Rh chemical shift have appeared in the literature[15] performed at the nonrelativistic GIAO-B3LYP level of theory on complexes bearing chelating bidentate phosphine ligands and N-donor ligands. A very good agreement was found with measured ^{103}Rh chemical shifts.

Calculations of NMR chemical shifts have, in general, proved to be very sensitive to geometry effects (see below). Thus, the concomitant need for predetermined structural information apparently limits any computational approach, especially when large molecules are considered. On the other hand, when experimental data are available for comparison, the calculations are helpful for gaining indirect information about the molecular structure in solution and the reactivity at the metal centre.

In this work, we report new experimental ^{103}Rh chemical shifts, $\delta(^{103}Rh)$, of mono- and bimetallic indacenyl rhodium complexes and compare them with the results of relativistic DFT calculations. The effect of the molecular and electronic structures of rhodium complexes on the calculated chemical shift is discussed, indicating how our computational protocol is efficient in predicting $\delta(^{103}Rh)$ accurately in small molecules and in giving precious information for larger systems where, as may be expected, a somewhat poorer correlation is found. Finally, for carbonyl compounds, the relation of the rhodium chemical shift with the HOMO–LUMO gap is discussed. Interestingly, the HOMO–LUMO transition is not the most important, and higher energy transitions involving low-lying orbitals give a large contribution to the paramagnetic term of the shielding constant.

Results and Discussion

We measured the ^{103}Rh NMR chemical shift of a series of rhodium(I) organometallic compounds synthesised in our laboratories. These are half-sandwich rhodium complexes in which the metal is coordinated to a cyclopentadienyl moiety, either a simple cyclopentadienyl ring or the cyclopentadienyl part of a larger spacer, as in the case of indenyl, *s*- and *as*-indacenyl bridges. The ancillary ligands can be CO, ethylene or 1,5-cyclooctadiene (cod). In the case of bimetallic complexes with *as*-indacenediide, two stereoisomers are available in which the inorganic groups are disposed on the same side (*syn*) or on opposite faces of the bridge (*anti*). The investigated systems are reported in Figure 1.

Chemical shifts of rhodium have been measured indirectly by using HMBC[4] between the olefin protons of the cod ligand and the ^{103}Rh atom ($J_{H-Rh} \approx 2$ Hz) for complexes **10**, **12**, **13** and **14**, and between the H atoms of the methyl group at the indacenyl 2-position and ^{103}Rh atom ($J_{H-Rh} \approx$

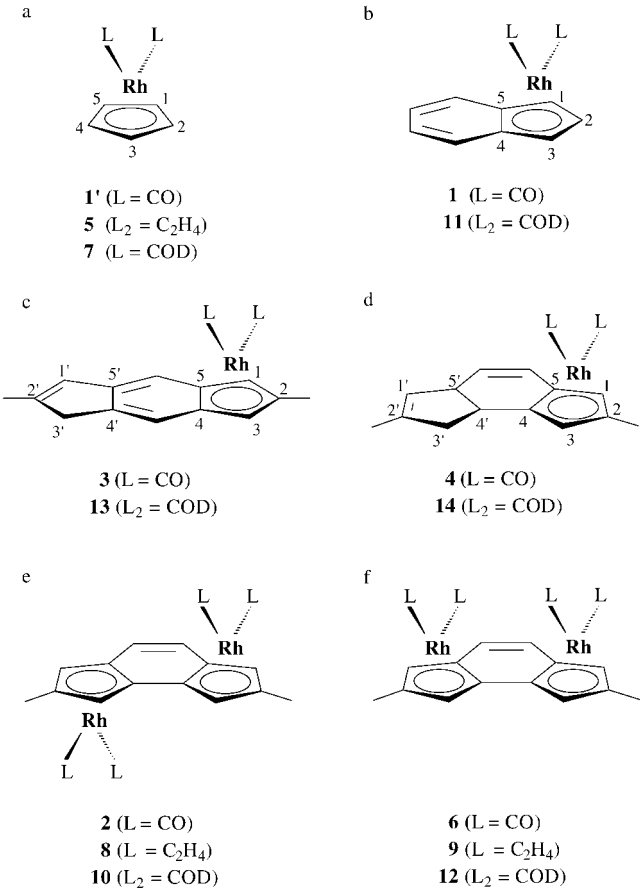

Figure 1. Experimentally studied mono- and bimetallic rhodium complexes **1**–**14**. Their data are listed in Table 1.

2 Hz) for complexes **2**, **3**, **4**, **6**, **8** and **9**. A typical two-dimensional heterocorrelated NMR spectrum is shown in Figure 2.

Due to the chemical similarity of the various complexes shown in Figure 1, their chemical shifts cover a relatively small range of 700 ppm. The experimental values are reported in Table 1, together with the calculated values that will be discussed later. In Table 2 we also report experimental chemical-shift data for a set of small complexes of rhodium shown in Figure 3; these data are taken from the literature, except for complex **4′** which has been measured. The data were compared with the results of our calculations in order to assess the validity of the computational approach.

Indacenyl complexes with CO ancillary ligands show the largest shielding, followed by ethylene complexes and finally cod complexes (Table 1). For the three pairs of *anti*/*syn* bimetallic complexes, **2**/**6**, **8**/**9** and **10**/**12**, the *anti* isomer is always more shielded by approximately 100 ppm. By considering the variation in chemical shift when the bridging ligand is changed (keeping the same ancillary ligands) a relationship might be established with the hapticity variation. For example, looking at the experimental $\delta(^{103}\mathrm{Rh})$ of the carbonyl derivatives **1′** and **1**, and of the cod derivatives **7** and **11**, it is evident that on changing from the cyclopentadienyl to indenyl spacer, the shielding of ^{103}Rh is progressively reduced. In order to quantify the hapticity we chose, for the sake of simplicity, the slip distortion parameter $\Delta = 0.5(\mathrm{M{-}C4} + \mathrm{M{-}C5}) - 0.5(\mathrm{M{-}C1} + \mathrm{M{-}C3})$[23] (carbon atom labels are indicated in Figure 1). The variation of ^{103}Rh chemical shifts with the slip distortion parameter, calculated on the basis of X-ray data of cod complexes, are represented graphically in Figure 4(I–III). For a more complete structural description, selected distances and angles of cod derivatives are summarised in Table 3. On the basis of the Δ values, rhodium is changing from a slightly distorted η^5 coordination in the cyclopentadienyl complex to a combination of $\eta^3+\eta^2$ in the indenyl cod derivative. Thus, the experimental ^{103}Rh chemical shifts reproduce the progres-

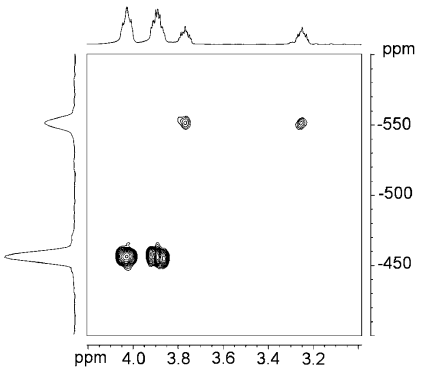

Figure 2. Inverse two-dimensional ^{1}H,^{103}Rh NMR spectrum of a mixture of *anti* and *syn* isomers of complexes **10** and **12**. Experimental conditions are described in the text. On top are the ^{1}H signals of the cod olefins, while on the left are the ^{103}Rh chemical shifts.

Table 1. Experimental chemical shifts, $\delta(^{103}\mathrm{Rh})$, and calculated shielding constants, σ, of the studied mono- and bimetallic rhodium complexes **1**–**14** (Figure 1). Experimental values are from this work, except for complexes **1**, **5**, **7** and **11**. All values are in ppm.

	δ_{expt}	δ_{calcd}[a,b]	$\Delta\delta$	σ_d[b]	σ_p[b]
[(indenyl)Rh(CO)$_2$] (**1**)	−1038[c]	−1079	41	4355	−4033
anti-[(2,7-dimethyl-*as*-indacenediide){Rh(CO)$_2$}$_2$] (**2**)	−1008	−1087[d]	79	4354	−4024
[(2,6-dimethyl-5-hydro-*s*-indacenide)Rh(CO)$_2$] (**3**)	−987	−1034	47	4354	−4077
[(2,7-dimethyl-8-hydro-*as*-indacenide)Rh(CO)$_2$] (**4**)	−972	−929	−43	4355	−4183
[(Cp)Rh(C$_2$H$_4$)$_2$] (**5**)	−945[e]	−1057	112	4351	−4051
syn-[(2,7-dimethyl-*as*-indacenediide){Rh(CO)$_2$}$_2$] (**6**)	−901	−972[d]	71	4354	−4139
[(Cp)Rh(cod)] (**7**)	−777[e]	−878	101	4350	−4229
anti-[(2,7-dimethyl-*as*-indacenediide){Rh(C$_2$H$_4$)$_2$}$_2$] (**8**)	−729	−859[d]	130	4348	−4246
syn-[(2,7-dimethyl-*as*-indacenediide){Rh(C$_2$H$_4$)$_2$}$_2$] (**9**)	−652	−808[d]	156	4348	−4297
anti-[(2,7-dimethyl-*as*-indacenediide){Rh(cod)}$_2$] (**10**)	−552	−590[d]	38	4355	−4522
[(indenyl)Rh(cod)] (**11**)	−487[f]	−448	−39	4350	−4659
syn-[(2,7-dimethyl-*as*-indacenediide){Rh(cod)}$_2$] (**12**)	−457	−603[d]	146	4355	−4509
[(2,6-dimethyl-5-hydro-*s*-indacenide)Rh(cod)] (**13**)	−421	−423	2	4349	−4683
[(2,7-dimethyl-8-hydro-*as*-indacenide)Rh(cod)] (**14**)	−399	−300	−99	4349	−4806
[(indenyl)Rh(CO)$_2$] (**1**)	−1038	−883[g]	−155	4355	−4326
[(2,6-dimethyl-5-hydro-*s*-indacenide)Rh(CO)$_2$] (**3**)	−987	−1244[g]	257	4354	−3964
anti-[(2,7-dimethyl-*as*-indacenediide){Rh(cod)}$_2$] (**10**)	−552	−64[g]	−488	4354	−5144
anti-[(2,7-dimethyl-*as*-indacenediide){Rh(cod)}$_2$] (**10**)	−552	−473[h]	−79	4351	−4732
syn-[(2,7-dimethyl-*as*-indacenediide){Rh(cod)}$_2$] (**12**)	−457	−770[h]	313	4350	−4434[i]
[(2,7-dimethyl-8-hydro-*as*-indacenide)Rh(cod)] (**14**)	−399	−180[h]	−219	4352	−5026

[a] The reference value for the chemical shift, −757 ppm, is taken from the intercept of the linear fit of Figure 4; [b] Relativistic scalar ZORA/TZP all-electrons except **4** and **7** for which a TZ2P basis set was used; [c] Experimental value taken from ref. [16]; [d] For bimetallic complexes the value is the average of the results obtained for the two centres; [e] Experimental value taken from ref. [3]; [f] Experimental value taken from ref. [16]; [g] Fully optimised structure. The reference value is in this case −854 ppm; [h] X-ray structure;[6] the employed reference value is −854 ppm; [i] A large difference between the two equivalent centres is calculated for σ_p as −4617 and −4251 ppm, respectively.

Table 2. Experimental and calculated chemical shifts, $\delta(^{103}\mathrm{Rh})$, for the rhodium complexes shown in Figure 3. All values are in ppm.

	δ_{expt}	σ_{calcd}[a]	δ_{calcd}	$\Delta\delta$	σ_{calcd}[b]	σ_{SO}[c]
[Rh(Cp)(CO)$_2$][d] (**1′**)	−1322	416	−1270	−52	807	388
[Rh(CO)]$_4^-$[e] (**2′**)	−644	−131	−723	79	286	409
[Rh(CO)$_2$Cl]$_2^-$[f] (**3′**)	84	−959	105	−21	−552	405
[Rh(cod)]$_2^+$ (**4′**)	677	−1597	743	−66	−1185	407
[Rh(acac)(C$_2$H$_4$)$_2$][g] (**5′**)	1170	−1950	1096	74	−1548	390
[RhI$_4$(SMe$_2$)$_2$]$^-$[h] (**6′**)	2958	−4342	3488	−530	−3374	793
[RhBr$_4$(SMe$_2$)$_2$]$^-$[h] (**7′**)	4532	−5443	4589	−57	−4785	639
[RhCl$_4$(SMe$_2$)$_2$]$^-$[h] (**8′**)	5226	−5918	5064	162	−5290	596
[Rh(acac)$_3$][i] (**9′**)	8358	−8063	7209	1149	−7478	508

[a] Relativistic scalar ZORA/TZ2P all-electrons; [b] Relativistic spin-orbit ZORA/TZ2P all-electrons; [c] Spin-orbit contribution to relativistic spin–orbit ZORA/TZ2P all-electrons. [d] Experimental value taken from ref. [17]; [e] Experimental value taken from ref. [18]; [f] Experimental value taken from ref. [19]; [g] Experimental value taken from refs. [9,20]; [h] Experimental values taken from ref. [21]; [i] Experimental value taken from ref. [22].

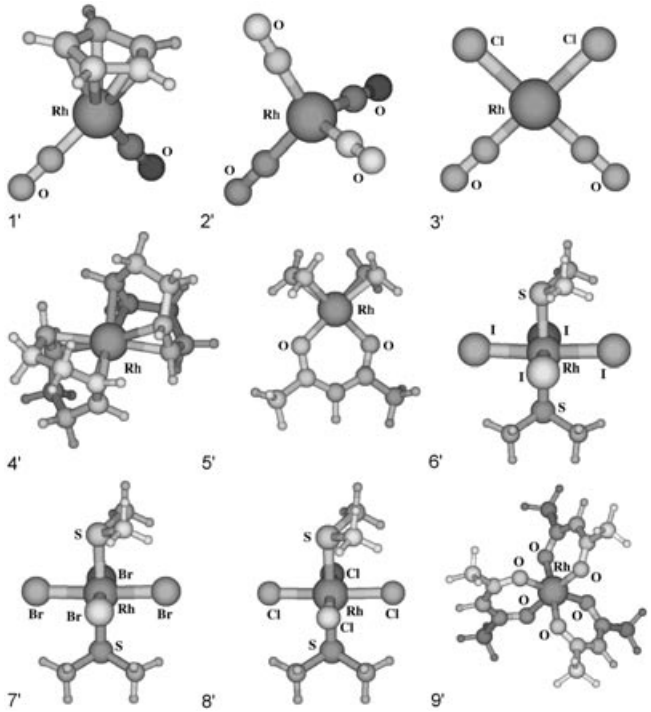

Figure 3. Structures of the molecules listed in Table 2. Shading level indicates depth and not atom type.

sive metal deshielding well for both cod and CO derivatives (Figure 4(I)). An interesting observation of Figure 4 is that the variation of the experimental chemical shifts with the slip distortion parameter exhibits the same trend and that the effect of the different ancillary ligands is simply a shift of the values.

DFT calculations of $\delta(^{103}Rh)$ for model rhodium complexes: Quantum-chemical methods allow the calculation of the shielding constant (σ), which can be written as the sum of a diamagnetic (σ_d) and a paramagnetic (σ_p) contribution, plus a spin–orbit term (σ_{SO}) in cases where spin–orbit coupling is explicitly considered in the theoretical treatment. Clearly, only the total shielding constant is physically observable, but such a breakdown may be quite instructive. The diamagnetic term is generally constant for a given nucleus in different compounds, because it depends mainly on the core-shell electrons, which are not involved in chemical bonding (therefore it cancels out in the chemical-shift calculation). The paramagnetic term can be written as the sum of two contributions (a detailed theoretical treatment can be found in ref. [27] and references therein): the first one, σ_p^{oc-oc}, is a sum over all pairs of occupied orbitals and is generally small; the second term, σ_p^{oc-vir}, is a sum over all pairs of occupied virtual orbitals; each term is weighted by the inverse of the energy gap and is proportional to the magnetic coupling between the two MOs involved.[27] This latter term (σ_p^{oc-vir}) gives by far the largest contribution to the paramagnetic term of the shielding constant (σ_p) and, being different in different compounds, is mostly responsible for the variation in chemical shift.

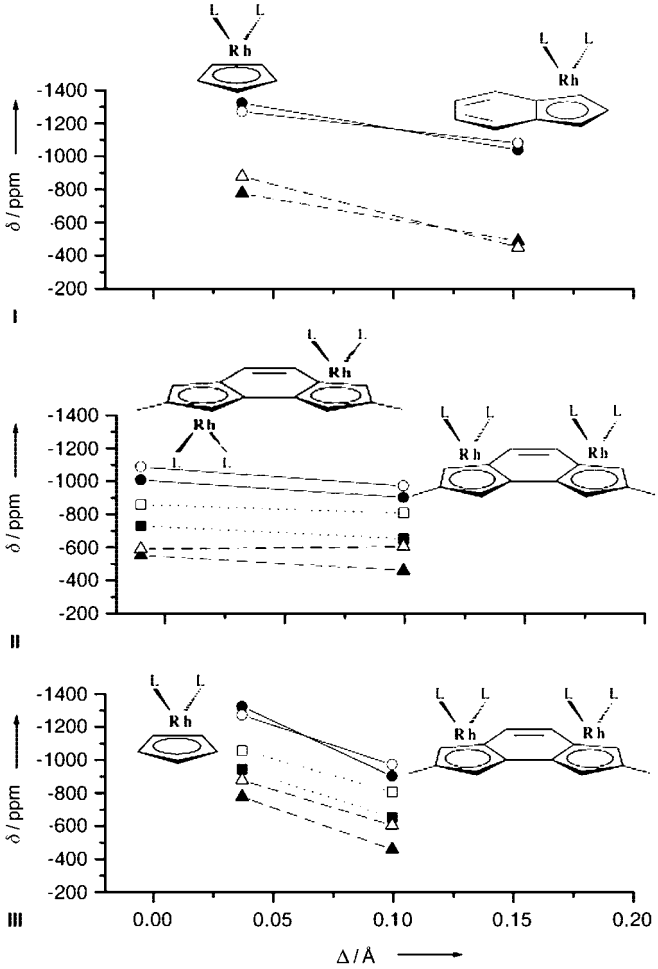

Figure 4. Changes in experimental (filled symbols) and calculated (empty symbols) chemical shifts with the slip distortion parameter Δ: cyclopentadienyl and indenyl complexes (I), *syn*- and *anti*-binuclear *as*-indacenyl complexes (II), cyclopentadienyl and *syn*-binuclear *as*-indacenyl complexes (III), with the ancillary ligands CO (circles), ethylene (squares) and cod (triangles). The horizontal axis is the same for each spectrum.

In order to test the accuracy and efficiency of the computational method we ran calculations for a set of small model molecules. These were selected for being small in order to save computational time, and for their simple and non-ambiguous structure, preferably free from conformational degrees of freedom. They were also chosen in order to cover a wide range of chemical shifts. As one can see in Figure 3 these complexes exhibit both various oxidation states and coordination geometries of rhodium. Model geometries were built and then fully optimised at the B3LYP level of theory (see computational details in the Experimental Section). Selected bond lengths and angles taken from X-ray data, when available, were compared with those from optimised geometries and are indicated in Table 4. When exactly matched structures were not found, similar complexes were considered. The agreement between calculated and crystallographic geometries is satisfactory.

For a straight comparison with experimental chemical shifts (δ_{expt}) we need to know the shielding constant of the reference compound (σ_{ref}). From these terms, the calculated

Table 3. Crystallographic and DFT-optimised selected bond lengths (Å), angles (°) and slip distortion parameters Δ (Å) of cod complexes.[a]

	7[b]	**10**[c]	**11**[d]	**12**[c]	**13**[e]	**14**[e]	**10**[f]
Rh1–C1	2.233(8)	2.277(8)	2.211	2.28(1)	2.187(7)	2.220(7)	*2.303*
Rh1–C2	2.265(7)	2.243(9)	2.245	2.24(1)	2.231(9)	2.249(7)	*2.328*
Rh1–C3	2.223(7)	2.28(1)	2.220	2.15(1)	2.228(9)	2.224(6)	*2.308*
Rh1–C4	2.278(8)	2.30(1)	2.373	2.30(1)	2.324(9)	2.375(6)	*2.540*
Rh1–C5	2.273(8)	2.252(9)	2.362	2.29(1)	2.365(8)	2.371(6)	*2.524*
Rh1–Q[g]	1.908	1.920	1.928	1.908	1.922	1.968	*2.062*
Rh1–M1[h]	2.110(7)	1.997	2.009	1.991	2.002	2.001	1.997
	2.039	*2.049*	*2.059*	*2.068*	*2.054*	*2.030*	*2.056*
Rh1–M2[h]	2.120(8)	2.007	2.005	1.922	2.013	2.022	2.007
	2.039	*2.043*	*2.062*	*2.045*	*2.068*	*2.070*	*2.044*
M1–Rh1–M2	87.2	87.8	87.6	86.1	87.5	87.3	87.8
	86.7	*86.7*	*86.9*	*86.4*	*86.9*	*87.1*	*87.6*
Δ	0.04	0.00[i]	0.15	0.08	0.14	0.15	*0.23*
Rh2–C1′		2.30(1)		2.20(1)			*2.332*
Rh2–C2′		2.28(1)		2.18(1)			*2.339*
Rh2–C3′		2.26(1)		2.25(1)			*2.286*
Rh2–C4′		2.288(8)		2.35(1)			*2.518*
Rh2–C5′		2.243(9)		2.33(1)			*2.526*
Rh2–Q′[g]		1.915		1.918			*2.061*
Rh2–M1′[h]		2.006		1.980			2.006
		2.046		*2.051*			*2.053*
Rh2–M2′[h]		1.997		1.995			1.997
		2.040		*2.043*			*2.041*
M1′–Rh2–M2′		87.3		86.9			87.3
		86.7		*86.5*			*87.1*
Δ		−0.02[i]		0.12			*0.21*

[a] Standard deviations, when available, are indicated. The X-ray and DFT distances Rh–Cp are equal because constrained geometry optimisations were performed; in the other cases DFT-calculated values are reported in italics; [b] X-ray structure taken from ref. [24]; [c] X-ray structure taken from ref. [6c]; [d] X-ray structure taken from ref. [25c]; [e] X-ray structure taken from ref. [6b]; [f] These data are referring to DFT fully optimised geometry; [g] Q and Q′ denote the centroids of the cyclopentadienyl moieties; [h] M1, M2, M1′ and M2′ denote the middle points of cod olefinic bonds; [i] Δ values were calculated referring to the couples of atoms C5–C6 (C5′–C6′) and C1–C3 (C1′–C3′), as for all complexes **7** and **11**–**14**. In complex **10**, zero and negative values are due to the fact that the distances Rh1–C5 and Rh2–C5′ are uncommonly short (ref. [26]) and the typical slippage towards C2 and C2′ is not encountered.

Table 4. Crystallographic and DFT-optimised selected bond lengths (Å) and angles (°) of complexes **1′**–**9′**.[a]

1′					**2′**	
Rh–C_{CO}	Rh–Q	Δ	C_{CO}–Rh–Q	Rh–C_{CO}–O	Rh–CO	C–Rh–C
1.808(2)[b]	1.936(2)[b]	0.018	135.1(1)	177.8(2)	1.96(6)[d]	105.5(26)[d]
1.855[c]	*2.017*[c]	*0.013*[c]	*134.2*[c]	*179.3*[c]	*1.949*	*109.5*
3′						
Rh–Cl1	Rh–Cl2	Rh–CO(1)	Rh–CO(2)	Cl1–Rh–Cl2	C1–Rh–C2	Rh–C1–O1
2.353(5)[e]	2.342(6)[e]	1.79(2)[e]	1.86(2)[e]	91.7(2)[e]	95.2(11)[e]	176.8(18)[e]
2.436	*2.435*	*1.859*	*1.859*	*94.1*	*95.3*	*179.6*
4′		**5′**				
Rh–M[f]	M–Rh–M′[f]	Rh–O	Rh–C1	Rh–C2	O–Rh–O	C1–Rh–C2
2.143[g]	84.5[g]	2.051(4)[h]	2.129(5)[h]	2.125(6)[h]	90.9(2)[h]	37.6(2)[h]
2.204	*83.6*	*2.073*	*2.169*	*2.169*	*90.9*	*37.5*
6′		**7′**		**8′**		**9′**
Rh–S	Rh–I	Rh–S	Rh–Br	Rh–S	Rh–Cl	Rh–O
2.302[l]	2.69[l]	2.302[l]	–	2.302[l]	2.251[l]	1.999[m]
2.449	*2.813*	*2.429*	*2.590*	*2.417*	*2.442*	*2.035*

[a] Standard deviations, when available, are indicated; DFT-calculated values are reported in italics; [b] From the X-ray structure of [Rh(Cp)(CO)(PPh_3)] (PIFREB);[28] [c] In this case from model DFT fully optimised structure; [d] From the X-ray structure of [$Rh_4(CO)_{12}$] (FOWTIU);[29] [e] From the X-ray structure (BOZWOC);[30] [f] M denotes the middle point of cod olefinic bonds; M–Rh–M′ indicates the angle formed by rhodium and the two middle points of the olefine bonds in a cod group; [g] From the X-ray structure (HUFQEE);[31] [h] From the X-ray structure;[15b] [i] From the X-ray structure of *trans*-[$Rh(CO)_2I_4$]$^-$;[32] [l] From the X-ray structure (CLMSRH);[33] [m] From the X-ray structure (ACACRH10).[34]

chemical shift, δ_{calcd}, is obtained as $\sigma_{ref}-\sigma$. Such a reference compound is missing for rhodium (see the Experimental Section) therefore we have obtained $-\sigma_{ref}$ directly from the intercept of the linear correlation between $-\sigma_{calcd}$ and δ_{expt}. The results are reported in Table 2. The correlation at the scalar ZORA/TZ2P level is very good, as shown in Figure 5 (the correlation coefficient is 0.999, the slope of the linear fit is 0.987 and σ_{ref} is −854 ppm), except for compounds **6′** and **9′** which are not included (ZORA = zeroth order regular approximation; TZ2P = (triple-ζ plus two polarizations). The deviation observed for compound **6′** is expected. In fact, when several heavy atoms, typically iodine, are bonded to a centre, strong spin–orbit coupling effects are observed.[35] A scalar relativistic approach is, therefore, unable of correctly describing the shielding at the central atom. However, such a deviation is totally recovered at the spin–orbit ZORA/TZ2P level of theory (Figure 5). Again, we observed the exception of compound **9′** which did not correlate so well with the experimental data. We repeated the calculation of the shielding constant of compound **9′** at the scalar ZORA/TZP level of theory (TZP = triple-ζ plus one polarization), freezing the distance Rh–O to the crystallographic value (see Table 4) and we obtained a poorer value, that is, $\sigma = -7236$ ppm. The reason for this slight disagreement, which also led us to test a different functional (see computational details in the Experimental Section), is unclear and will not be investigated further.

The results obtained with the smaller basis set, TZP, still at the scalar relativistic level, are almost indistinguishable from those obtained with the

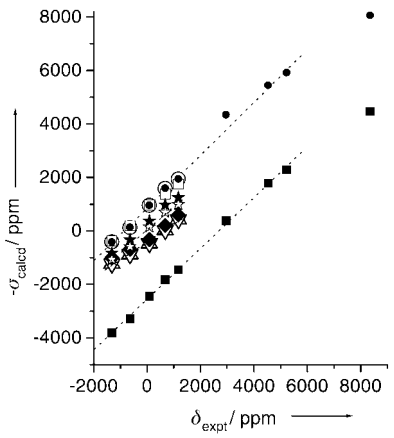

Figure 5. Correlation between the experimental chemical shift, δ_{expt}, of ^{103}Rh and the negative calculated shielding constants, $-\sigma_{calcd}$, in the compounds shown in Figure 4. ● = sc(≡scalar ZORA)/TZ2P with linear fit ($a+bx$), not including **6′** and **9′**, $a = 854$, $b = 0.987$, $R = 0.999$; ○ = sc/TZP; □ sc/DZ; ☆ = sc/TZP Rh·3d frozen core with linear fit, $a = 40$, $b = 0.860$, $R = 0.997$; ★ = nonrelativistic/TZP Rh·3d frozen core; △ = sc/TZ2P Rh·4p frozen core with linear fit, $a = -413$, $b = 0.664$, $R = 0.994$; ▽ = sc/TZP Rh·4p frozen core; ◆ = nonrelativistic/TZP Rh·4p frozen core; ■ = spin–orbit/TZ2P with linear fit, not including **9′**, $a = 451$, $b = 0.949$, $R = 0.999$; the data points at this level of theory are displaced by −3000 ppm for clarity.

larger TZ2P level (see Table 5). This important finding allows us to safely use the less-expensive TZP basis set for the calculation of the Rh shielding constant in the large mono- and bimetallic complexes. The agreement is worse when the relatively small DZ (DZ = double-ζ) basis set is employed. The correlation coefficient is still rather good (0.994) but the slope of the linear fit is now 0.862. The use of frozen-core basis sets, especially for the heavy atom Rh has also been investigated. In Figure 5 and Table 5 we also show the data obtained for a basis set with a frozen core up to 3d and 4p electrons for rhodium, and an all-electrons basis set for the other atoms. As we see, a systematic underestimation of the shielding constant is calculated by freezing the core electrons up to the 3d and 4p levels. In fact, the slope of the linear fit is only 0.869 and 0.664, respectively.

Finally, we have calculated the shielding constant at the nonrelativistic level, still with a frozen-core basis set for rhodium (all-electrons basis sets for rhodium, and many other heavy atoms are only available for ZORA relativistic calculation in ADF). Apart from the known systematic error due to the use of frozen-core basis sets, the correlation appears to be somewhat worse compared with the results at the scalar relativistic level. This result is expected for a second-row transition metal such as rhodium.

Therefore, the result of this set of calculations is that a qualitative correlation for the chemical shift of ^{103}Rh can be obtained even with small and/or frozen-core basis sets. For a more quantitative result, an all-electrons TZP basis set is at least recommended. Scalar relativistic effects also need to be taken into account. In fact, for heavy transition metals such as rhodium, the relativistic contraction of the s and p inner electron orbitals has large effects on the diamagnetic part of the shielding constant and indirectly affects d and f orbitals, an expansion effect which is in turn reflected in σ_p.[3]

The spin–orbit coupling contribution to the shielding constant is rather large. However, it is roughly constant for most compounds, therefore it cancels out in the calculation of the chemical shift, δ_{calcd}. If we are interested only in obtaining a tool for a quantitative prediction of the ^{103}Rh chemical shift in various compounds, the contribution coming from spin–orbit coupling can be ignored. A similar conclusion was drawn in ref. [36] for xenon compounds. Of course, spin–orbit coupling cannot be ignored if more than one heavy nucleus, typically iodine, is bonded to rhodium, as in compound **6′**, in which the spin–orbit contribution to the shielding constant is about twice as large as that in other compounds with ligands containing only light atoms.

Table 5. Calculated shielding constants (σ) at different levels of theory for some of the rhodium complexes shown in Figure 3. All values are in ppm.

	σ_{calcd}[a]	σ_{calcd}[b]	σ_{calcd}[c]	σ_{calcd}[d]	σ_{calcd}[e]	σ_{calcd}[f]	σ_{calcd}[g]
$[Rh(Cp)(CO)_2]$ (**1′**)	409	361	1226	1227	1011	1070	832
$[Rh(CO)]_4^-$ (**2′**)	−126	−194	866	881	685	592	334
$[Rh(CO)_2Cl]_2^-$ (**3′**)	−955	−968	466	468	327	−147	−371
$[Rh(cod)]_2^+$ (**4′**)	−1585	−1385	−32	−27	−201	−697	−975
$[Rh(acac)(C_2H_4)_2]$ (**5′**)	−1940	−1748	−435	−427	−598	−987	−1245

[a] Relativistic scalar ZORA/TZP all-electrons; [b] Relativistic scalar ZORA/DZ all-electrons; [c] Relativistic scalar ZORA/TZ2P rhodium frozen core, Rh·4p; [d] Relativistic scalar ZORA/TZP rhodium frozen core, Rh·4p; [e] Nonrelativistic/TZP rhodium frozen core, Rh·4p; [f] Relativistic scalar ZORA/TZP rhodium frozen core, Rh·3d; [g] Nonrelativistic/TZP rhodium frozen core, Rh·3d.

DFT calculations of $\delta(^{103}Rh)$ for half-sandwich cyclopentadienyl, indenyl and indacenyl rhodium complexes: We now turn our attention to the experimentally studied mono- and bimetallic compounds **1**–**14**, as shown in Figure 1.

The shielding constants have been calculated at the relativistic scalar ZORA/TZP all-electrons level of theory, except for compounds **4**–**7** for which the TZ2P basis set was used (see Table 1). The results of the bimetallic complexes are estimated as the average of the two rhodium atoms, which, because of small geometrical distortions, may not be perfectly equivalent. The correlation between experimental and calculated values is shown in Figure 6. The correlation coefficient is 0.961, the slope of the linear fit is 1.073 and σ_{ref} is −757 ppm. The average deviation of calculated chemical shifts from the experimental values is 82 ppm, with the largest of all being 156 ppm. This is a rather good result if we keep in mind 1) the neglect of conformational effects in the calculation, and 2) the large dependence of the chemical shift on the structure; in the present treatment, we also neglected solvent effects because no coordination phenomena of the solvent are believed to

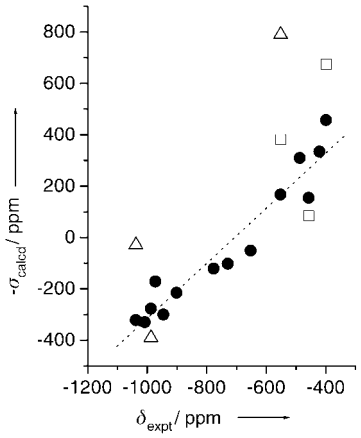

Figure 6. Correlation between the experimental and calculated chemical shift of ^{103}Rh in the studied mono- and bimetallic complexes: ● = geometries optimised with constrains with linear fit $a+bx$: $a=757$, $b=1.073$, $R=0.961$; □ = X-ray geometries; △ = optimisation with no constrains.

occur. However, despite the difference in chemical shift among our various Rh complexes being quite small (with all the values being within just 700 ppm) some general trends of the experimental results are well reproduced by the calculations (see Figure 4(I–III)).

Of paramount importance seems to be the effect of using the wrong geometry for a calculation of NMR chemical shifts: Bühl[15d] investigated the influence of the geometry by computing the metal shift for several fixed rhodium–ethylene distances in [Rh(acac)(C_2H_4)$_2$] and found a large dependence of the $\delta(^{103}Rh)$ on the Rh–C bond length (more than 100 ppm per 0.01 Å). In the half-sandwich rhodium complexes, the relevant geometrical parameters which mostly affect $\delta(^{103}Rh)$ are the distance Rh–Cp, the metal hapticity and the spatial disposition of the ancillary ligands. Therefore special care was needed in optimising the geometries of our complexes. X-ray data are available only for cod derivatives (see Table 3). The geometries of CO and ethylene complexes were obtained by starting from the backbone of the analogue cod derivative and substituting the ancillary ligands. The accuracy of this assumption was further supported through a search in the Cambridge structural database.[37] X-ray data of indacenyl-bridged rhodium complexes are only available with the ancillary ligand cod; however, numerous structures include the rhodium–cyclopentadienyl and rhodium–indenyl units. In most cases the former exhibits almost perfect η^5 coordination. For example, Δ is 0.018 Å in [Rh(CO)(Cp)(PPh_3)] (PIFREB),[28] 0.033 Å in (η^5-cyclopentadienyl)(η^2-ethene)(η^2-1,2-diphenylethene)rhodium (XISYUT),[38] 0.039 Å in (η^5-cyclopentadienyl)(η^2-ethene)(η^2-tetrafluoroethylene)rhodium (CPEFRH),[39] and 0.011 Å in (η^5-cyclopentadienyl)(η^2-ethene)(η^2-sulphur dioxide)rhodium (CPSXER).[40] A search of rhodium indenyl complexes gave 79 structures, for which the slip distortion parameter can vary by about 0.08 Å. For example, Δ is 0.200(7) Å in dicarbonyl(η^5-indenyl)rhodium (VATYUK),[23] 0.205(5) in dicarbonyl(η^5-4,5,6,7-tetramethylindenyl)rhodium (KUWPOH),[23] but decreases to 0.186 Å in (–)-dicarbonyl(η^5-2-menthyl-4,7-dimethylindenyl)rhodium (MIFFIQ).[41] The Δ value is 0.161 Å in bis(η^2-ethylene)(η^5-indenyl)rhodium,[42] 0.168 Å in (–)-bis(η^2-ethylene)(η^5-2-menthyl-4,7-dimethylindenyl)rhodium (MORCOL)[43] and 0.118 Å in [μ_2-2-(η^5-cyclopentadienyl)-2-(η^5-indenyl)propane]bis[bis(η^2-ethylene)]dirhodium (POZTIH).[44] Finally, Δ is 0.152 Å in (η^4-cod)(η^5-indenyl)rhodium(HAPPET),[5c] but decreases to 0.122 Å in (η^4-cycloocta-1,5-dienyl)(η^5-2-menthyl-4,7-dimethylindenyl)rhodium (MORCIF)[43] and to 0.116 Å in (–)-(η^4-cycloocta-1,5-dienyl)(η^5-2-menthylindenyl)rhodium (MORCEB).[43] The Δ values extracted from the cod derivatives' backbones and also imposed by us to CO and ethylene cyclopentadienyl indenyl and indacenyl complexes (Table 3) are acceptable distortion parameters falling in the range of those measured in structurally similar ethylene and carbonylated compounds.

We then optimised all geometries keeping the five distances rhodium–carbon frozen, thus maintaining a fixed position of rhodium with respect to the coordinated cyclopentadienyl moiety of the spacer. In fact, nonconstrained geometry optimisations of {Rh(cod)} derivatives, at the B3LYP/LANL2DZ,6-31G** level of theory with Gaussian 98, lead to a noticeable displacement of rhodium from its crystallographic position;[26] for example, calculated distortion slip parameters of fully optimised **10** are 0.23 and 0.21, as reported in Table 3. Keeping the Rh–cyclopentadienyl moiety frozen means that no hapticity variations were allowed in the calculations, that is, the crystallographic position of rhodium in the cod derivatives is assumed to persist also in solution. This choice turned out to be adequate, since the correlation between calculated and experimental chemical shifts is quite good.

The coordination mode of rhodium is crucial for determining the complex reactivity, as a hapticity reduction corresponds to an increase in the electrophilicity of the metal centre, occuring as a consequence of the electron density on the metal diminishing.[45] In particular, in the case of indenyl and indacenyl ligands, the slippage of the metal from an η^5 to an $\eta^3+\eta^2$ bonding mode may induce an increase in the aromatic character of the benzene ring and the simultaneous disruption of the aromaticity of the five-membered ring to form an allylene electronic structure of higher energy. The slippage of the rhodium atom in these polycyclic, aromatic bridged complexes is also accompanied by the folding of the cyclopentadienyl moiety, as expected in the presence of relevant contributions coming from an η^3-bonding mode.[45] Hapticity changes should be clearly reflected in $\delta(^{103}Rh)$, as small changes in the coordination sphere usually result in significant changes in the paramagnetic contribution of the chemical shift for transition-metal nuclei.[16]

Most of the results for the smaller monometallic complexes are in better agreement with experimental values than those for the larger bimetallic complexes. Chemical-shift differences for pairs of homologous compounds are rather well reproduced: for the *anti* complexes, the calculated $\Delta\delta$(**10**,**8**) and $\Delta\delta$(**10**,**2**) are 269 and 497 ppm, respectively (experimental: 177 and 456 ppm), while for the *syn* isomers the relative calculated values $\Delta\delta$(**12**,**9**) and $\Delta\delta$(**12**,**6**) are 205 and 369 ppm, respectively (experimental: 195 and 444 ppm). Therefore, the decrease in shielding of the Rh nucleus as

the ancillary ligands are changed from CO to ethylene and finally cod, is correctly reproduced for both *syn* and *anti* isomers at a semiquantitative level (see Figure 4).

In Figure 6 and Table 1 we also show the chemical shift of rhodium for complexes **10**, **12** and **14** calculated using the X-ray structures, and for complexes **1**, **3**, **5** and **10** obtained after a full geometry optimisation. As we have already mentioned, if no constrains are imposed during the geometry optimisation, the position of rhodium with respect to the bridging ligand changes dramatically towards a more pronounced η^3 coordination and the distance with respect to the cyclopentadienyl moiety increases[26] (see Table 3). As a result, the calculated chemical shift for these geometries largely disagrees with the experimental value. We have studied complex **5** in more detail. From gas-phase electron diffraction data, the distance between rhodium and the centroid of the cyclopentadienyl moiety is known to be 1.907(3) Å.[46] We performed free and constrained geometry optimisations varying this distance, that is, slightly increasing and decreasing the experimental value (see Table 6). The calculated chemical shifts for the wrong geometries are in large disagreement with the experimental values. In contrast, at the experimental distance a good agreement is found. This further confirms the importance of the distance between the rhodium and cyclopentadienyl centroid in these organometallic complexes.

Indeed, as already noted in ref. [36], the results from the calculation of NMR properties at this level of theory can be taken as indicators of the correctness of a given structure. On the other hand, the results of the calculations on the few available X-ray structures also appear to be less well correlated than constrained optimised structures. This indicates that a certain structural relaxation takes place in solution; in particular, being that the hapticity is the same in X-ray and DFT-optimised geometries, this mainly involves the conformation of the ancillary ligands. In Table 7 we have reported selected bond lengths and angles to describe rhodium coordination to the ancillary ligands CO and ethylene, taken both from X-ray data and DFT-optimised structures.

We have shown how crystallographic hapticity changes are reflected in $\delta(^{103}Rh)$, as we observed a progressive measured and calculated downfield shift on going from cyclopentadienyl derivatives to indenyl-monometallic complexes. This is due to a major contribution or availability of a less-shielded and coordinatively unsaturated 16-electron rhodium centre, which is commonly correlated to an increased reactivity of the complex.

In the case of bimetallic *as*-indacenediide bridged species, the comparison with monometallic analogous complexes is not straightforward because the electronic distribution in

Table 6. Calculated chemical shifts for complex **5** (Figure 1) at selected rhodium–cyclopentadienyl distances. All values are in ppm.

Rh–Q[a] [Å]	σ_d	σ_p	δ_{calcd}	$\Delta\delta$
2.018	4351	−4496	−612	−333
2.006[b]	4351	−4451	−754	−191
1.907	4351	−4051	−1057	112
1.863	4351	−3882	−1226	281

[a] Q indicates the centroid of the cyclopentadienyl ring; [b] Fully optimised geometry.

Table 7. Selected bond distances (Å) and angles (°) of DFT-optimised CO and ethylene half-sandwich rhodium complexes and analogous crystallographic parameters in complexes of similar structure.[a]

	Rh–C1[b]	Rh–C2[b]	C1–Rh–C2	Rh–C1–O1	Rh–C2–O2
1	*1.898*	*1.899*	*93.2*	*178.4*	*178.4*
3	*1.903*	*1.895*	*93.4*	*178.3*	*177.9*
4	*1.904*	*1.879*	*93.1*	*178.9*	*179.0*
	Rh1–C1[b]	Rh1–C2[b]	C1–Rh1–C2	Rh1–C1–O1	Rh1–C2–O2
2	*1.891*	*1.890*	*91.5*	*179.2*	*179.5*
6	*1.889*	*1.893*	*91.7*	*179.0*	*179.2*
	Rh2–C1′[b]	Rh2–C2′[b]	C1′–Rh2–C2′	Rh2–C1′–O1′	Rh2–C2′–O2′
2	*1.890*	*1.891*	*91.6*	*179.4*	*179.8*
6	*1.899*	*1.891*	*92.0*	*178.7*	*176.4*
	Rh–C1[c]	Rh–C2[c]	Rh–C3[c]	Rh–C4[c]	M_{12}–Rh–M_{34}[d]
5	*2.159*	*2.158*	*2.172*	*2.173*	*95.1*
	Rh1–C1[c]	Rh1–C2[c]	Rh1–C3[c]	Rh1–C4[c]	M_{12}–Rh1–M_{34}[d]
8	*2.164*	*2.170*	*2.163*	*2.175*	*95.4*
9	*2.167*	*2.174*	*2.155*	*2.183*	*94.6*
	Rh2–C1′[c]	Rh2–C2′[c]	Rh2–C3′[c]	Rh2–C4′[c]	$M_{1'2'}$–Rh2–$M_{3'4'}$[d]
8	*2.169*	*2.165*	*2.159*	*2.176*	*95.4*
9	*2.195*	*2.195*	*2.149*	*2.183*	*95.6*
	Rh–C1[b]	Rh–C2[b]	C1–Rh–C2	Rh–C1–O1	Rh–C2–O2
1[e]	*1.894*	*1.894*	*94.5*	*178.4*	*178.4*
3[e]	*1.890*	*1.890*	*94.5*	*178.4*	*178.4*
	Rh–C1[b]	Rh–C2[b]	C1–Rh–C2	Rh–C1–O1	Rh–C2–O2
a[f]	1.866(5)	1.857(5)	92.2(2)	179.5(5)	178.2(5)
b[g]	1.861(2)	1.865(3)	90.19(11)	178.0(3)	177.8(3)
	Rh–C1[c]	Rh–C2[c]	Rh–C3[c]	Rh–C4[c]	M_{12}–Rh–M_{34}[d]
c[h]	2.15(2)	2.13(2)	2.14(2)	2.15(2)	–
d[i]	2.127(3)	2.147(3)	2.145(3)	2.148(3)	95.2

[a] Standard deviations, when available, are indicated; DFT-calculated values are reported in italics; [b] C1–C2 and C1′–C2′ are the carbon atoms of the CO ligands; [c] C1–C4 and C1′–C4′ are the carbon atoms of the ethylene ligands; [d] M_{ij} indicates the middle point of the olefine bond C*i*-C*j*; [e] DFT fully optimised structures; [f] From X-ray structure of dicarbonyl(η^5-4,5,6,7-tetramethylindenyl)rhodium (KUWPOH);[23] [g] From X-ray structure of (−)-dicarbonyl(η^5-2-menthyl-4,7-dimethylindenyl)rhodium (MIFFIQ);[41] [h] From X-ray structure of (η^5-$CpCMe_2C_9H_7$)Rh(C_2H_4)$_2$;[44] [i] From X-ray structure of (−)-bis(η^2-ethylene)(η^5-2-menthyl-4,7-dimethylindenyl)rhodium (MORCOL).[43]

the metal environment is very different in *as*-indacenide and *as*-indacenediide derivatives. For example, in the case of **10** and **14**, two distinct orientations of the ancillary ligand cod are mainly controlled by the electronic structure of the spacer.[26]

Concerning the bimetallic complexes, the existence of two stereoisomers allows interesting considerations (see Figure 4(II)). In solution a single signal is observed for each bimetallic species since the environment of the two rhodium nuclei is equivalent; $\delta(^{103}\mathrm{Rh})$ of *anti* complexes **2**, **8** and **10** is shifted about 100 ppm highfield with respect to that of the *syn* complexes **6**, **9** and **12**. A more pronounced η^3 character in Rh−Cp bonding is expected in the *syn* complexes, also on the basis of crystallographic data and is due mainly to steric reasons: in an attempt to counterbalance the hindrance of the two adjacent inorganic groups, both rhodium centres slip away and the *as*-indacenediide bridge strongly bends losing its aromaticity. Calculated $\Delta\delta$(**2**,**6**) and $\Delta\delta$(**8**,**9**) are in very good agreement with the experimental values. In contrast, calculated $\Delta\delta$(**10**,**12**) does not reflect the expected trend. We believe this can be ascribed to geometry effects. In fact, in contrast to the *anti* conformer **10**, calculated $\delta(^{103}\mathrm{Rh})$ of the *syn* conformer **12** does not correlate well with the experimental value (Figure 4). In its optimised molecular structure, in agreement with X-ray data, the two ancillary ligands cod have nonequivalent orientations. This is reflected in the two distant values of the calculated $\delta(^{103}\mathrm{Rh})$ for the two adjacent nuclei. In this case, the average value poorly describes the true rhodium environment in solution and confirms that the sensitivity of the metal chemical shift is due to subtle geometry variations.[47]

Analysis of the paramagnetic shielding constant: A qualitative understanding of the variations of the chemical shift and how these are affected by the electronic structure of the complex, in particular by the presence of different ancillary ligands, can be gained by breaking down the $\sigma_p^{oc\text{-}vir}$ contribution into its separate components, following ref. [27]. We start our analysis with $[Rh(Cp)(CO)_2]$ (**1′**): The contribution coming from the occupied virtual orbitals is by far the dominant term since it accounts for the large paramagnetic contribution to the shielding constant. The most important terms of the sum over all the occupied virtual transitions are reported in Table 8. The sum is very slowly convergent because, for example, after including the ten most important contributions, there is still a difference of about 1000 ppm in the value of $\sigma_p^{oc\text{-}vir}$ (−3562 ppm). However, a qualitative analysis can be made by inspection of the few terms reported in Table 8. The most important transition contributing to the paramagnetic shielding constant is the HOMO−4→ LUMO. The HOMO−4 is essentially a rhodium d orbital, a nonbonding MO, while the LUMO is a combination of rhodium d orbitals with a relatively small contribution of ligand p orbitals. The situation is therefore very similar to the case of ferrocene discussed in ref. [27]. Essentially the same can be said for the second most important contribution to the paramagnetic shielding term. A qualitatively different situation is, instead, observed for the third most important contribution shown in Table 8. The transition is characterised by a very large energy gap. Therefore, there is intrinsically strong magnetic coupling between the two MOs involved. The HOMO−16 is a bonding orbital between the d_{yz} rhodium orbital and the carbonyl p_z orbitals (that is along the CO axes), while the LUMO+2 is an antibonding orbital between the rhodium d_{z^2} and $d_{x^2-y^2}$ with the p orbitals localised on the carbonyl moiety. This strong magnetic interaction seems to be characteristic of carbonylated species. In fact, it is absent in complex **7**, [Rh(Cp)(cod)], also reported in Table 8. It gives an additional contribution to the shielding of rhodium in complexes with carbonyl ligands: without this strong magnetic coupling between a low-energy bonding MO and an antibonding MO, rhodium in carbonyl complexes would be even more deshielded.

Table 8. Contribution to the shielding constant for some selected examples.[a] All values of σ are in ppm.

			σ	σ_d	σ_p	$\sigma_p^{oc\text{-}vir}$	ΔE_{oc-vir} [eV]
1′			1011	4397	−3386	−3562	2.52[b]
HOMO−4	→	LUMO				−789	4.91
HOMO−1	→	LUMO+1				−417	4.02
HOMO−16	→	LUMO+2				−299	10.07
7			824	4389	−3565	−4063	2.62[b]
HOMO−2	→	LUMO				−1524	3.65
HOMO−1	→	LUMO+1				−421	4.57
HOMO	→	LUMO				−269	2.62
4			818	4396	−3578	−3683	2.46[b]
HOMO−6	→	LUMO				−620	4.84
HOMO	→	LUMO				−277	2.46
HOMO−3	→	LUMO				−247	4.06
HOMO−2	→	LUMO+1				−196	3.58
HOMO−28	→	LUMO+3				−177	10.16
12			329	4388	−4058	−4508	2.60[b]
HOMO−3	→	LUMO				−917	3.43
HOMO−3	→	LUMO+1				−513	3.58
HOMO−1	→	LUMO				−255	2.60

[a] Nonrelativistic scalar ZORA/TZP Rh frozen core Rh·4p; [b] HOMO–LUMO gap.

A very similar qualitative picture emerges from the analysis of the results of [(2,7-dimethyl-8-hydro-*as*-indacenide)-$Rh(CO)_2$], complex **4**. This is not surprising because the local environment of rhodium resembles that of complex **1′**. A contribution from a high-energy transition is also present, being the fifth contribution to the paramagnetic shielding constant in order of magnitude. The occupied and virtual orbitals involved in this high-energy transition for **4** are the same as for **1′** and are shown in Figure 7.

The case of the cod complex **14** is somewhat similar to the model complex **7**. The most important contributions, all involving frontier orbitals, are mainly from d rhodium orbitals. There is no contribution coming from a high-energy transition, in contrast to the case of carbonyl derivatives. Nevertheless, the chemical shift of rhodium in cod derivatives is shifted to higher fields by roughly 500 ppm. Often, the value of the paramagnetic contribution, σ_p, is correlated with the HOMO–LUMO energy gap, but in our case this gap is essentially the same for the four complexes investigated. However, the HOMO–LUMO transition is not the most important transition for these rhodium complexes; a similar behaviour was observed in a study on platinum complexes.[48] If we look at the energy gap of the most important

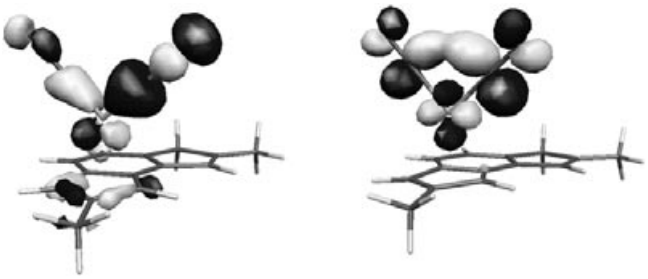

Figure 7. Molecular orbitals of the high-energy transition at the nonrelativistic TZP level Rh·4p frozen core, which contribute to the paramagnetic shielding term in complex **4**. Left: HOMO−28; Right: LUMO+3.

transitions contributing to the paramagnetic shielding term we see, for the cod derivatives, that it is smaller than the corresponding term in the carbonylated complexes: this is the reason why rhodium appears to be more shielded in the former complexes.

Conclusion

A relativistic, DFT computational protocol has been established to calculate NMR shielding constants of ^{103}Rh nuclei. A very good correlation was obtained over the full range of chemical-shift values. The method was employed to calculate the metal chemical shift of mono-Rh^{I}-*s*- and -*as*-hydroindacenide derivatives and bis-Rh^{I}-*as*-indacenediide complexes for a direct comparison with the corresponding experimental values presented here. A satisfactory agreement was found when the geometries were optimised by keeping the Rh–Cp distance fixed to the X-ray value in order to avoid changes in hapticity, while the other conformational degrees of freedom were allowed to relax. This was possible for cod derivatives for which X-ray data was available, while for the other derivatives, the X-ray Rh–Cp distance of the analogous cod derivative was used. The agreement becomes much poorer if the non-optimised X-ray structures are used or a full, unconstrained optimisation is performed. This suggests that while the hapticity of Rh in solution is almost unchanged compared with the solid state, the overall geometry of the molecule is indeed different due to the relaxation of crystal-packing effects.

The effect of different ancillary ligands (CO, cod, C_2H_4) has been discussed; in particular, the breakdown of the paramagnetic part of the shielding constant in carbonyl and cyclooctadienyl analogous complexes revealed that the biggest contributions involve magnetic coupling of mainly metal d-based MOs, but that in general the HOMO–LUMO coupling is not the most important. Moreover, in carbonylated complexes there is strong coupling between a low-energy occupied MO and a virtual MO, in the absence of which, $\delta(^{103}\mathrm{Rh})$ in these species would be shifted even more high-field. The calculations also reproduced the trend due to the hapticity differences reasonably well, and in the case of carbonylated and ethylene Rh-*as*-indacenediide derivatives, permitted a clear distinction between the two stereoisomers *syn* and *anti*. We believe that the strongest limitation to a more precise calculation of $\delta(^{103}\mathrm{Rh})$ for large and polynuclear complexes is the geometry, since model or crystallographic structures can be very different from the molecule in solution. In these cases, the calculations point out the necessity of taking conformational effects into account for a complete picture of the electronic structure of the compound of interest and its consequent reactivity.

Studies on shielding/reactivity correlations are in progress. A possible extension to catalytic systems, providing the opportunity to screen potential homogeneous catalysts by determining their ^{103}Rh chemical shift, could have a beneficial impact on structural and synthesis-oriented organometallic chemistry.

Experimental Section

General procedures: All reactions and complex manipulations were performed in an oxygen-free atmosphere. The solvents were carefully dried and deoxygenated before use. The complexes are microcrystalline, air-stable powders.

The synthesis and characterisation of all bimetallic complexes and monometallic species with cod (1,5-cyclooctadiene) as the ancillary ligand have been previously described.[6] The [(2,7-dimethyl-6-hydro-*as*-indacenide)Rh(CO)$_2$] and [(2,6-dimethyl-5-hydro-*s*-indacenide)Rh(CO)$_2$] were obtained by bubbling CO through a solution of the analogous Rh(cod) derivative in THF (dried and deoxygenated) at −20 °C for two hours. Extraction of the reaction mixture with hexane gave the expected product in an almost quantitative yield.

[(2,7-Dimethyl-6-hydro-*as*-indacenide)Rh(CO)$_2$]: ^{1}H NMR (CD_2Cl_2, TMS, 298 K): $\delta = 7.146$ and 6.910 (*AB* quartet, 2H, $J_{AB} = 7.6$ Hz; H5 and H4, respectively), 6.604 (m, 1H; H8), 5.755 (m, 1H; H1), 5.811 (m, 1H; H3), 3.313 and 3.219 (*AB* quartet, 2H, $J_{AB} = -18$ Hz; H6$_{exo}$ and H6$_{endo}$, respectively), 2.276 (d, 3H, $J(^{103}\mathrm{Rh}{-}\mathrm{H}) = 2.2$ Hz; 2-CH_3), 2.207 ppm (s, 3H; 7-CH_3); ^{13}C NMR (CD_2Cl_2, TMS, 298 K): $\delta = 191.48$ (d, $J(^{103}\mathrm{Rh}{-}\mathrm{C}) = 86$ Hz; CO), 147.65 (C7), 139.68 (C8a), 135.13 (C5a), 124.55 (C8), 120.92 (C5), 117.14 (C4, C2), 115.38 (C1a), 110.17 (C3a), 74.64 (C3), 74.12 (C1), 43.74 (C6), 16.81 (7-CH_3), 16.25 ppm (2-CH_3).

[(2,6-Dimethyl-5-hydro-*s*-indacenide)Rh(CO)$_2$]: ^{1}H NMR (CD_2Cl_2, TMS, 298 K): $\delta = 7.124$ (m, 1H; H8), 6.934 (m, 1H; H4), 6.408 (m, 1H; H7) 5.723 (m, 1H; H3), 5.707 (m, 1H; H1), 3.215 (s, 2H; H5), 2.245 (d, 3H, $J(^{103}\mathrm{Rh}{-}\mathrm{H}) = 2.2$ Hz; 2-CH_3), 2.110 ppm (s, 3H; 6-CH_3); ^{13}C NMR (CD_2Cl_2, TMS, 298 K): $\delta = 190.61$ (d, $J(^{103}\mathrm{Rh}{-}\mathrm{C}) = 17.51$ Hz; CO), 147.00 (C6), 144.15 (C4a), 141.09 (C7a), 127.35 (C7), 117.89 (C3a), 115.94 (C2), 115.29 (C8a), 113.37 (C4), 108.36 (C8), 76.60 (C1, C3), 42.34 (C5), 17.02 (6-CH_3), 16.26 ppm (2-CH_3).

^{103}Rh NMR: All ^{103}Rh NMR spectra (CD_2Cl_2, 300 K) were recorded on a Bruker Avance DRX spectrometer operating at 400.13 MHz, using a 5 mm inverse low-frequency probe head with a *z*-gradient coil (90°(^{1}H) = 7.50 μs, 90°(^{103}Rh) = 7 μs). The HMBC experiments were carried out by using the following sequence: D1–90°(^{1}H)–$^1/_2J$–90°(^{103}Rh)–t_1/2-GP1–D16-180°(^{1}H)–GP2–D16–t_1/2–90°(^{103}Rh)–GP3–D16–ACQ. Acquisition parameters D1 = 1 s, $^1/_2J = 0.1$ s, D16 = 0.2 ms, GP = 1 ms, 64 scans were acquired per t_1 increment, block size 2048 × 512 points for experiment, gradient amplitude: GP1:GP2:GP3 = 70.1:30:43.3 G cm^{-1}. After zero-filling in F1, the 2048 × 2048 matrix was transformed by applying a Qsine weighing function. The spectral width for ^{103}Rh was 5000 ppm; the spectral width for ^{1}H was 10 ppm. The $\delta(^{103}\mathrm{Rh})$ values are in ppm and were calculated by determining the absolute frequency of the cross peak and relating it to the arbitrary reference frequency (Ξ = 3.16 MHz at 100.00 MHz), which is 12.64 MHz for operation at 400.13 MHz ^{1}H frequency. Acquisition time: 13 h. The concentration of the samples was 6×10^{-2} M.

Computational details: All geometries were optimised at the B3LYP/LANL2DZ-ECP[49] level for Rh, 6-31G** for light atoms (H, C and S) and 6-311G** for the halogens (Cl, Br and I) with the software package Gaussian 98.[50] Density functional calculations were run with the ADF

code[13] using the Becke–Perdew functional[51] at the nonrelativistic level of theory, scalar relativistic ZORA level and spin–orbit ZORA level. Various Slater basis sets have been tested: DZ, TZP and TZ2P all-electrons; TZP frozen core up to 3d for rhodium (Rh·3d and all-electrons for the light atoms); TZP and TZ2P frozen core up to 4p for rhodium (Rh·4p and all-electrons for the light atoms). The result of the calculation is the shielding tensor, $\boldsymbol{\sigma}$, whose isotropic component, σ, is considered. The majority of the calculations have been carried out with the NMR module of the ADF package[52,53] and some with the EPR module of ADF,[52] which allows, at the nonrelativistic level, the breakdown of the shielding tensor into various contributions and therefore permits a qualitative interpretation of the chemical shift.[27] A different functional, PBE (Perdew–Burke–Ernzerhof),[54] was tested. The shielding constants of complexes **1′**–**5′** were calculated at the scalar relativistic ZORA/TZP level of theory. The correlation with the experimental chemical shifts is almost undistinguishable from that obtained at the same level of theory using the Becke–Perdew functional and complex **9′** deviates significantly also in this case. These data are provided in the Supporting Information.

Acknowledgement

All the calculations have been run on the IBM SP4 of the CINECA Supercomputing Centre, Italy. We thank Prof. Alessandro Bagno (Università di Padova) for helpful discussions. We are grateful to Ileana Menegazzo (Università di Padova) and Anna Minoja (Bruker BioSpin) for technical support. We are also grateful to Dr. Franco Benetollo (ICIS-CNR, Padova) for kind assistance in consulting the Cambridge structural database.

[1] a) *Rhodium Catalyzed Hydroformylation* (Eds.: P. W. N. M. Van Leeuwen, C. Claver), Kluwer Academic, Dordrecht, **2000**; b) R. S. Dickson, *Homogeneous Catalysis with Compounds of Rhodium and Iridium (Catalysis by Metal Complexes)*, Vol. *8*, Reidel, Dordrecht, **1985**.

[2] a) M. D. Ward, *Acc. Chem. Res.* **1998**, *31*, 842; b) M. D. Ward, *Chem. Soc. Rev.* **1995**, *24*, 121.

[3] a) C. J. Jameson, in *Multinuclear NMR* (Ed.: J. Mason), Plenum, London, **1987**; b) *Transition Metal Nuclear Magnetic Resonance* (Ed.: P. S. Pregosin), Elsevier, Amsterdam, **1991**; c) R. Benn, A. Rufinska, *Angew. Chem.* **1986**, *98*, 851–871; *Angew. Chem. Int. Ed. Engl.* **1986**, *25*, 861–881.

[4] T. D. W. Claridge, *High-Resolution NMR Techniques in Organic Chemistry*, Pergamon, Oxford, **1999**, Chapter 6, p. 245.

[5] a) A. Ceccon, A. Gambaro, S. Santi, G. Valle, A. Venzo, *Chem. Commun.* **1989**, 52; b) A. Ceccon, A. Gambaro, S. Santi, A. Venzo, *J. Mol. Catal.* **1991**, *69*, L1; c) C. Bonifaci, A. Ceccon, A. Gambaro, P. Ganis, S. Santi, G. Valle, A. Venzo, *Organometallics* **1993**, *12*, 4211; d) C. Bonifaci, A. Ceccon, A. Gambaro, P. Ganis, L. Mantovani, S. Santi, A. Venzo, *J. Organomet. Chem.* **1994**, *475*, 267; e) C. Bonifaci, A. Ceccon, A. Gambaro, P. Ganis, S. Santi, G. Valle, A. Venzo, *J. Organomet. Chem.* **1995**, *492*, 35; f) C. Bonifaci, G. Carta, A. Ceccon, A. Gambaro, S. Santi, A. Venzo, *Organometallics* **1996**, *15*, 1630; g) L. Mantovani, A. Ceccon, A. Gambaro, S. Santi, P. Ganis, A. Venzo, *Organometallics* **1997**, *16*, 2682; h) C. Amatore, A. Ceccon, S. Santi, J. N. Verpeaux, *Chem. Eur. J.* **1997**, *3*, 279; i) C. Amatore, A. Ceccon, S. Santi, J. N. Verpeaux, *Chem. Eur. J.* **1999**, *5*, 3357; j) S. Santi, A. Ceccon, L. Crociani, A. Gambaro, P. Ganis, M. Tiso, A. Venzo, A. Bacchi, *Organometallics* **2002**, *21*, 565; k) S. Santi, F. Benetollo, A. Ceccon, L. Crociani, A. Gambaro, P. Ganis, M. Tiso, A. Venzo, *Inorg. Chim. Acta* **2003**, *344*, 221.

[6] a) C. Bonifaci, A. Ceccon, A. Gambaro, F. Manoli, L. Mantovani, P. Ganis, S. Santi, A. Venzo, *J. Organomet. Chem.* **1998**, *557*, 97; b) A. Bisello, A. Ceccon, A. Gambaro, P. Ganis, F. Manoli, S. Santi, A. Venzo, *J. Organomet. Chem.* **2000**, *593–594*, 315–324; c) A. Ceccon, A. Bisello, L. Crociani, A. Gambaro, P. Ganis, F. Manoli, S. Santi, A. Venzo, *J. Organomet. Chem.* **2000**, *600*, 94; d) A. Ceccon, P. Ganis, F. Manoli, A. Venzo, *J. Organomet. Chem.* **2000**, *601*, 267; e) S. Santi, A. Ceccon, F. Carli, L. Crociani, A. Bisello, M. Tiso, A. Venzo, *Organometallics* **2002**, *21*, 2679.

[7] a) J. M. Manriquez, M. D. Ward, W. M. Reiff, J. C. Calabrese, N. L. Jones, P. J. Carroll, E. E. Bunel, J. S. Miller, *J. Am. Chem. Soc.* **1995**, *117*, 6182; b) P. Roussel, D. R. Cary, S. Barlow, J. C. Green, F. Vartet, D. O'Hare, *Organometallics* **2000**, *19*, 1071; c) P. Roussel, J. M. Drewitt, D. R. Cary, C. G. Webster, D. O'Hare, *Chem. Commun.* **1998**, 2055; d) D. R. Cary, C. G. Webster, M. J. Drewitt, S. Barlow, J. C. Green, D. O'Hare, *Chem. Commun.* **1997**, 953; e) D. R. Cary, J. C. Green, D. O'Hare, *Angew. Chem.* **1997**, *109*, 2730–2733; *Angew. Chem. Int. Ed. Engl.* **1997**, *36*, 2618–2620; f) S. Barlow, D. R. Cary, M. J. Drewitt, D. O'Hare, *J. Chem. Soc. Dalton Trans.* **1997**, 3867; g) W. L. Bell, C. J. Curtis, A. Medianer, C. W. Eigenbrot, Jr., R. Curtis Haltiwanger, C. G. Pierpont, J. C. Smart, *Organometallics* **1988**, *7*, 691.

[8] a) M. Koller, W. Von Philipsborn, *Organometallics* **1992**, *11*, 467; b) V. Tedesco, W. Von Philipsborn, *Organometallics* **1995**, *14*, 3600.

[9] B. Akermark, M. R. A. Blomberg, J. Glaser, L. Öhrström, S. Wahlberg, K. Wärnmark, K. Zetterberg, *J. Am. Chem. Soc.* **1994**, *116*, 3405.

[10] W. Von Philipsborn, *Chem. Soc. Rev.* **1999**, *28*, 95.

[11] R. G. Parr, W. Yang, *Density Functional Theory of Atoms and Molecules*, Academic Press, Oxford, **1989**.

[12] J. Autschbach, T. Ziegler, in *Relativistic Computation of NMR Shieldings and Spin–Spin Coupling Constants*: *Encyclopedia of Nuclear Magnetic Resonance*, *Vol. 9: Advances in NMR* (Eds.: D. M. Grant, R. K. Harris), Wiley, Chichester, **2002**. (A review article specifically dealing with heavy-atom NMR computations).

[13] G. te Velde, F. M. Bickelhaupt, E. J. Baerends, C. Fonseca Guerra, S. J. A. van Gisbergen, J. G. Snijders, T. Ziegler, *J. Comput. Chem.* **2001**, *22*, 931; http://www.scm.com.

[14] a) G. Schreckenbach, *Theor. Chem. Acc.* **2002**, *108*, 246; b) G. Schreckenbach, *Inorg. Chem.* **2002**, *41*, 6560; c) G. Schreckenbach, S. K. Wolff, T. Ziegler, *J. Phys. Chem. A* **2000**, *104*, 8244; d) R. Bouten, E. J. Baerends, E. van Lenthe, L. Visscher, G. Schreckenbach, T. Ziegler, *J. Phys. Chem. A* **2000**, *104* 5600; e) J. Autschbach, T. Ziegler, *Coord. Chem. Rev.* **2003**, *238–239*, 83.

[15] a) M. Bühl, *Organometallics* **1997**, *16*, 261; b) M. Bühl, M. Hakansson, A. H. Mahmoudkhani, L. Öhrström, *Organometallics* **2000**, *19*, 5589; c) J. G. Donkervoort, M. Bühl, J. M. Ernsting, C. J. Elsevier, *Eur. J. Inorg. Chem.* **1999**, 27; d) W. Leitner, M. Bühl, R. Fornika, C. Six, W. Baumann, E. Dinjus, M. Kessler, C. Krüger, A. Rufinska, *Organometallics* **1999**, *18*, 1196; e) M. Bühl, M. Kaupp, O. L. Malkina, V. G. Malkin, *J. Comput. Chem.* **1999**, *20*, 91.

[16] A. Ceccon, C. J. Elsevier, J. M. Ernsting, A. Gambaro, S. Santi, A. Venzo, *Inorg. Chim. Acta* **1993**, *204*, 15.

[17] a) P. B. Graham, M. D. Rausch, K. Täschler, W. Von Philipsborn, *Organometallics* **1991**, *10*, 3049; b) E. Maurer, S. Rieker, M. Schollbach, A. Schwenk, T. Egolf, W. Von Philipsborn, *Helv. Chim. Acta* **1982**, *65*, 26; c) P. B. Graham, M. D. Rausch, *Organometallics* **1991**, *10*, 3049.

[18] C. Brown, B. T. Heaton, L. Longhetti, W. T. Povey, D. O. Smith, *J. Organomet. Chem.* **1980**, *192*, 99.

[19] K. Timmer, D. H. M. V. Thewissen, J. W. Marsmann, *Recl. Trav. Chim. Pays-Bas* **1988**, *107*, 248.

[20] B. Akermark, J. Glaser, L. Öhrström, K. Zetterberg, *Organometallics* **1991**, *10*, 733.

[21] S. J. Anderson, J. R. Barnes, P. L. Goggin, R. J. Goodfellow, *J. Chem. Res. Synop.* **1978**, *286–287*, 3601.

[22] K. D. Grüninger, A. Schwenk, B. E. Mann, *J. Magn. Reson.* **1980**, *41*, 354.

[23] A. K. Kakkar, N. J. Taylor, T. B. Marder, J. K. Shen, N. Hallinan, F. Basolo, *Inorg. Chim. Acta* **1992**, *198–200*, 219.

[24] H. Adams, N. A. Bailey, B. E. Mann, B. F. Taylor, C. White, P. Yavari, *J. Chem. Soc. Dalton Trans.* **1987**, *8*, 1947.

[25] A. K. Kakkar, S. F. Jones, N. J. Taylor, S. Collins, T. B. Marder, *Chem. Commun.* **1989**, 1454.

[26] L. Orian, P. Ganis, S. Santi, A. Ceccon, submitted to *Phys. Chem. Chem. Phys.*

[27] G. Schreckenbach, *J. Chem. Phys.* **1999**, *110*, 11936.

[28] M. G. Choi, T. L. Brown, *Inorg. Chem.* **1993**, *32*, 5603.

[29] C. H. Wei, *Inorg. Chem.* **1969**, *8*, 2384.

[30] J. P. Farr, M. M. Olmstead, F. E. Wood, A. L. Balch, *J. Am. Chem. Soc.* **1983**, *105*, 792.
[31] L. Dahlenburg, N. Osthoff, F. W. Heinemann, *Acta Crystallogr. Sect. E* **2001**, *57*, 117.
[32] J. J. Daly, F. Sanz, D. Forster, *J. Am. Chem. Soc.* **1975**, *97*, 2551.
[33] V. I. Sokol, V. N. Nikolaev, M. A. Porai-Koshits, A. P. Kochetkova, L. B. Sveshnikova, *Koord. Khim.* **1975**, *1*, 675.
[34] J. C. Morrow, E. B. Parker, Jr., *Acta Crystallogr. Sect. B* **1973**, *29*, 1145.
[35] a) M. Kaupp, O. L. Malkina, V. G. Malkin, P. Pyykkö, *Chem. Eur. J.* **1998**, *4*, 118; b) M. Kaupp, O. L. Malkina, V. G. Malkin, *Chem. Phys. Lett.* **1997**, *265*, 55; c) V. G. Malkin, O. L. Malkina, D. R. Salahub, *Chem. Phys. Lett.* **1996**, *261*, 335.
[36] A. Bagno, G. Saielli, *Chem. Eur. J.* **2003**, *9*, 1486.
[37] *The Cambridge Structural Database: A Quarter of a Million Crystal Structures and Rising*; F. H. Allen, *Acta Crystallogr. Sect. B* **2002**, *58*, 380.
[38] H. Wadepohl, A. Metz, H. Pritzkow, *Chem. Eur. J.* **2002**, *8*, 1591.
[39] L. J. Guggenberger, R. Cramer, *J. Am. Chem. Soc.* **1972**, *94*, 3779.
[40] R. R. Ryan, P. G. Eller, G. J. Kubas, *Inorg. Chem.* **1976**, *15*, 797.
[41] H. Schumann, O. Stenzel, S. Dechert, F. Girgsdies, J. Blum, D. Gelman, R. L. Halterman, *Eur. J. Inorg. Chem.* **2002**, 211.
[42] M. Mlekuz, P. Bougeard, B. G. Sayer, M. J. McGlinchey, C. A. Rodger, M. R. Churchill, J. W. Ziller, S. K. Kang, T. A. Albright, *Organometallics* **1986**, *5*, 1656.
[43] H. Schumann, O. Stenzel, S. Dechert, F. Girgsdies, R. L. Halterman, *Organometallics* **2001**, *20*, 5360.
[44] P. Escarpa Gaede, P. H. Moran, A. N. Richarz, *J. Organomet. Chem.* **1998**, *559*, 107.
[45] a) L. F. Veiros, *J. Organomet. Chem.* **1999**, *587*, 232; b) M. J. Calhorda, C. A. Gamelas, I. S. Gonçalves, E. Herdtweck, C. C. Romão, L. F. Veiros, *Organometallics* **1998**, *17*, 2597; c) M. J. Calhorda, V. Felix, L. F. Veiros, *Coord. Chem. Rev.* **2002**, *230*, 49; d) M. J. Calhorda, L. F. Veiros, *Coord. Chem. Rev.* **1999**, *185–186*, 37.
[46] R. Blom, D. W. H. Rankin, H. E. Robertson, R. N. Perutz, *J. Chem. Soc. Dalton Trans.* **1993**, 1983.
[47] a) W. Koch, M. C. Holthausen, *A Chemist's Guide to Density Functional Theory*, 2nd ed., Wiley-VCH, Weinheim, **2001**, Chapter 11, p. 201; b) M. Bühl, in *Encyclopedia of Computational Chemistry* (Editor-in-Chief: P. von R. Schleyer), Wiley, Chichester, **1998**.
[48] T. M. Gilbert, T. Ziegler, *J. Phys. Chem. A* **1999**, *103*, 7535.
[49] a) A. D. Becke, *J. Chem. Phys.* **1996**, *104*, 1040; b) C. Lee, W. Yang, R. G. Parr, *Phys. Rev. B* **1988**, *37*, 785; c) P. J. Hay, W. R. Wadt, *J. Chem. Phys.* **1985**, *82*, 270; d) P. J. Hay, W. R. Wadt, *J. Chem. Phys.* **1985**, *82*, 284; e) P. J. Hay, W. R. Wadt, *J. Chem. Phys.* **1985**, *82*, 299; f) J. V. Ortiz, P. J. Hay, R. L. Martin, *J. Am. Chem. Soc.* **1992**, *114*, 2736; g) P. C. Hariharan, J. A. Pople, *Theor. Chim. Acta* **1973**, *28*, 213; h) M. N. Glukhovtsev, A. Pross, M. P. McGrath, L. Radom, *J. Chem. Phys.* **1995**, *103*, 1878; Basis sets were obtained from the *Extensible Computational Chemistry Environment Basis Set Database*, Version 4/17/03, as developed and distributed by the Molecular Science Computing Facility, Environmental and Molecular Sciences Laboratory which is part of the Pacific Northwest Laboratory, P.O. Box 999, Richland, WA 99352, USA, and funded by the U.S. Department of Energy. The Pacific Northwest Laboratory is a multiprogram laboratory operated by Battelle Memorial Institue for the U.S. Department of Energy under contract DE-AC06-76RLO 1830. Contact David Feller or Karen Schuchardt for further information.
[50] Gaussian 98 (Revision A.11.3), M. J. Frisch, G. W. Trucks, H. B. Schlegel, G. E. Scuseria, M. A. Robb, J. R. Cheeseman, V. G. Zakrzewski, J. A. Montgomery, Jr., R. E. Stratmann, J. C. Burant, S. Dapprich, J. M. Millam, A. D. Daniels, K. N. Kudin, M. C. Strain, O. Farkas, J. Tomasi, V. Barone, M. Cossi, R. Cammi, B. Mennucci, C. Pomelli, C. Adamo, S. Clifford, J. Ochterski, G. A. Petersson, P. Y. Ayala, Q. Cui, K. Morokuma, D. K. Malick, A. D. Rabuck, K. Raghavachari, J. B. Foresman, J. Cioslowski, J. V. Ortiz, B. B. Stefanov, G. Liu, A. Liashenko, P. Piskorz, I. Komaromi, R. Gomperts, R. L. Martin, D. J. Fox, T. Keith, M. A. Al-Laham, C. Y. Peng, A. Nanayakkara, C. Gonzalez, M. Challacombe, P. M. W. Gill, B. G. Johnson, W. Chen, M. W. Wong, J. L. Andres, M. Head-Gordon, E. S. Replogle, J. A. Pople, Gaussian, Inc., Pittsburgh, PA, **2002**.
[51] a) A. D. Becke, *Phys. Rev. A* **1988**, *38*, 3098; b) J. P. Perdew, *Phys. Rev. B* **1986**, *33*, 8822.
[52] a) G. Schreckenbach, T. Ziegler, *J. Phys. Chem.* **1995**, *99*, 606; b) G. Schreckenbach, T. Ziegler, *Int. J. Quantum Chem.* **1996**, *60*, 753.
[53] a) S. K. Wolff, T. Ziegler, *J. Chem. Phys.* **1998**, *109*, 895; b) S. K. Wolff, T. Ziegler, E. van Lenthe, E. J. Baerends, *J. Chem. Phys.* **1999**, *110*, 7689.
[54] J. P. Perdew, K. Burke, M. Ernzerhof, *Phys. Rev. Lett.* **1996**, *77*, 3865.

Received: October 29, 2003
Revised: March 16, 2004
Published online: June 30, 2004

